NANO LETTERS

2007
Vol. 7, No. 10
3041−3045

Highly Conductive Coaxial SnO_2–In_2O_3 Heterostructured Nanowires for Li Ion Battery Electrodes

Dong-Wan Kim,* In-Sung Hwang, S. Joon Kwon, Hae-Yong Kang, Kyung-Soo Park, Young-Jin Choi, Kyoung-Jin Choi, and Jae-Gwan Park

Nano-Science Research Division, Korea Institute of Science and Technology, Seoul 136-791, Korea

Received June 25, 2007

ABSTRACT

Novel SnO_2–In_2O_3 heterostructured nanowires were produced via a thermal evaporation method, and their possible nucleation/growth mechanism is proposed. We found that the electronic conductivity of the individual SnO_2–In_2O_3 nanowires was 2 orders of magnitude better than that of the pure SnO_2 nanowires, due to the formation of Sn-doped In_2O_3 caused by the incorporation of Sn into the In_2O_3 lattice during the nucleation and growth of the In_2O_3 shell nanostructures. This provides the SnO_2–In_2O_3 nanowires with an outstanding lithium storage capacity, making them suitable for promising Li ion battery electrodes.

Much effort has been made to overcome the numerous challenges associated with the design of one-dimensional (1D) nanostructures with well-controlled size, phase purity, crystallinity, and chemical composition, due to their fascinating properties and unique applications.[1,2] Furthermore, the preparation of 1D nanorods and nanowires with axially and radially modulated compositions has led to multiple functionalities by combining the physical properties of the different materials.[3−6] The synthesis of multicomponent 1D nano-heterostructures has been demonstrated using vapor, solution, template, lithographic, solid−solid, electrospinning, and assembly methods for applications in nanoelectronics, photonics, sensing, and catalysis.[7−11]

Additionally, inorganic 1D nanostructures are potentially useful as electrodes for Li-ion batteries, because the small size of these structures is usually correlated with their high surface area and large surface-to-volume ratio, which favors the physical or chemical interactions of the electrodes and lithium ions.[12−16] The benefits of enhanced active sites and short diffusion distances, which arise from 1D nanostructures, will thus result in a high capacity and fast kinetics.

Tin oxide (SnO_2) has been proposed as one of a family of alternative anode materials with a high storage capacity (theoretical value 781 mA h/g), but the practical use of this material has been frustrated by its fast capacity fading upon cycling, due to the severe volume changes that occur during lithium uptake and removal.[17,18] More recently, SnO_2 1D nanostructures such as nanowires/rods and nanotubes have been suggested for the purpose of obtaining improved cycling performance.[19−21] However, the design and lithium reactivity of 1D nano-heterostructures have rarely been studied.

In this Letter, we report the one-step preparation of SnO_2 nanowires with coaxially grown In_2O_3 overlayers. The growth mechanisms of the 1D core−shell heterostructure were also studied in detail. Furthermore, we demonstrate that this unique SnO_2−In_2O_3 nanowire heterostructure is a promising electrode for Li-ion batteries, because the surface modification of the SnO_2 nanowires by In_2O_3 leads to their having a high electronic conductivity during cycling, thereby improving the electrochemical performance.

The thermal evaporation process was employed to synthesize SnO_2−In_2O_3 nanowire heterostructures on n-type (100) Si substrates with a 3 nm thick gold coating. High-purity (99.99%) Sn and In metal powders thoroughly mixed at a weight ratio of 9:1 were used as the evaporation sources. This source material was placed on an alumina boat and loaded into the middle of a quartz tube (22 mm i.d., 800 mm length) placed in a horizontal electrical furnace. The temperature at the center of quartz tube which was initially under vacuum (∼0.05 Torr) was 750 °C, and then a constant flow of oxygen was maintained at a rate of 10 sccm for 20 min. Uniform nanowires were collected from the downstream substrates. The nanowires were characterized using X-ray powder diffraction (XRD, model M18XHF, Macsicence Instruments, Japan), Raman spectroscopy (model T64000, Horiba Jovin Yvon, France), field emission scanning electron microscopy (FESEM, model JSM-6330F, JEOL, Japan), and high-resolution transmission electron microscopy (HRTEM, model JEM-3000F, JEOL, Japan). The electrical transport properties were studied on devices consisting of individual

* To whom correspondence should be addressed. E-mail: dongwan1@empal.com.

10.1021/nl0715037 CCC: $37.00
Published on Web 08/31/2007

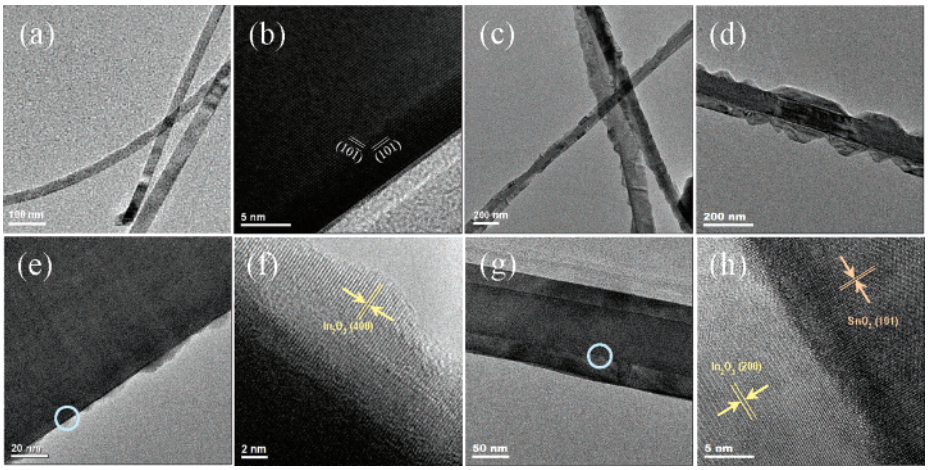

Figure 1. (a) Low-magnification TEM image of pure SnO_2 nanowires. The magnified image (b) shows the high crystallinity of the SnO_2 nanowire. (c) Typical TEM image of $SnO_2-In_2O_3$ nanowires. (d), (e), and (g) TEM images showing different shell nanostructures of $SnO_2-In_2O_3$ nanowires. (f) and (h) HRTEM images of the magnified views of the interfaces between the core and shell in (e) and (g), respectively.

nanowires. The nanowires were dispersed onto an n-type heavily doped Si substrate capped with a 300 nm thick silicon dioxide layer. Predefined alignment marks on the substrate were used to locate the position of the nanowires. After poly(methyl methacrylate) was spin coated onto the substrate as an electron-beam (e-beam) resist, e-beam lithography processes were used to define pairs of metal electrodes based on the nanowire's position, followed by Ti/Au (20/80 nm) metallization and liftoff. $I-V$ measurements were performed using an HP 4140B.

For the electrochemical evaluation of the $SnO_2-In_2O_3$ nanowire heterostructures, positive electrodes were prepared by mixing together 2−3 mg of the $SnO_2-In_2O_3$ nanowires, Super P (MMM Carbon, Brussels, Belgium) carbon black, and Kynar 2801 (PVdF-HFP) binder at a mass ratio of 70:18:12. Swagelok-type cells using Li metal foil, which were used as the negative electrode, and a separator film of Celgard 2400 were assembled and saturated with the liquid electrolyte, 1 M $LiPF_6$, in ethylene carbonate and dimethyl carbonate (1:1 by volume).[22] The assembled cells were galvanostatically cycled between 3.0 and 0.01 V using a Toyo system automated tester (TOSCAT-3100, Toyo System Co., Ltd., Fukushima, Japan).

The as-grown samples showed a high yield of nanowires covering the whole substrate surfaces. Figure 1 gives an overview of the typical TEM images of the as-synthesized $SnO_2-In_2O_3$ nanowires. For comparison, the images of the pure SnO_2 nanowires that were fabricated without an indium source under the same conditions are also shown in panels a and b of Figure 1. The SnO_2 nanowires were found to be ~50 nm in diameter with high crystallinity and a smooth surface. However, the surface of the $SnO_2-In_2O_3$ nanowires was relatively rough along the nanowire axis (Figure 1c). An irregular overlayer developed on most of the $SnO_2-In_2O_3$ nanowires, as shown in Figure 1d. Additionally, we observed a few nanowires having discrete anisotropic nanoclusters onto their surface (Figure 1e) and a thicker shell with a uniform diameter (Figure 1g). This outer axial growth along the core nanowire seems to depend on the reaction kinetics. More interestingly, the corresponding core and shell are indexed to be tetragonal SnO_2 and cubic In_2O_3, based on the lattice fringes in panels f and h of Figure 1. Further HRTEM investigations revealed the existence of an SnO_2/In_2O_3 core/shell heterostructure (Figure S1 of the Supporting Information).

Recently, it was reported that In_2O_3-beaded SnO_2 nanowires could be synthesized by the thermal evaporation of SnO at 600 °C and the subsequent carbothermal reduction of In_2O_3 at 900 °C.[23,24] However, the simultaneous formation of core/shell nanowires, which might occur due to the differences in the reactivities of the core and shell materials, has rarely been studied. The proposed nucleation and growth mechanisms for the formation of the $SnO_2-In_2O_3$ heterostructure are explained in detail below.

In the case of the vapor-phase transport in situ growth governed by the vapor−solid−liquid (VLS) growth mechanism of the nanowires formed from the two different precursors in this study, the priority of the inner part of the wire is determined by the body diffusion time of each precursor into the catalytic metal nucleus, t_{bi} ($i = 1, 2, x$, where the subscripts 1, 2, and x indicate SnO_2, In_2O_3, and $(In_2O_3)_x(SnO_2)_{1-x}$, respectively). The body diffusion time of In_2O_3 (t_{b2}) is about 2−3 times longer than that of SnO_2 (t_{b1}).[25] Moreover, the surface diffusion time on the catalytic metal nucleus, t_{si} ($i = 1, 2, x$), is much longer than t_{bi} in the event of the nanowire having a nanoscale radius.[26] Therefore, the formation of the inner part of the nanowire comprised of SnO_2 prior to the formation of In_2O_3 or $(In_2O_3)_x(SnO_2)_{1-x}$ alloy (or Sn-doped In_2O_3) hinges on the following inequalities such that $t_{b1} \ll t_{s1}$, $t_{b1} < t_{b2}$, and $t_{b1} < t_{bx}$. The resulting structure is the SnO_2 nanowire (here, the structure was assumed to be cylindrical), and in the VLS mechanism, its growth direction and radius are determined by the crystallinity of the materials and the size of the metal nucleus, respectively.[27,28] Furthermore, we could not observe any noticeable In_2O_3 nanowire growth under the same fabrication conditions with only the indium source.

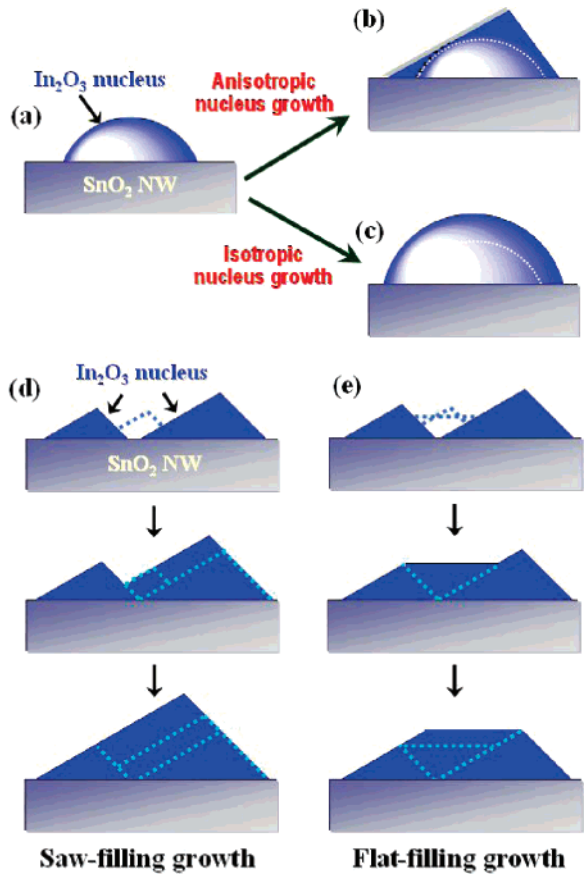

Figure 2. Schematic representation of (a) In_2O_3 nucleus on the SnO_2 core. The growth of the In_2O_3 nucleus can be achieved in (b) an anisotropic manner or (c) an isotropic manner. The In_2O_3 nuclei grown in an isotropic manner are transformed into (d) larger anisotropic nuclei satisfying a saw-filling growth mechanism or (e) an outer shell around the SnO_2 core satisfying the flat-filling growth mechanism.

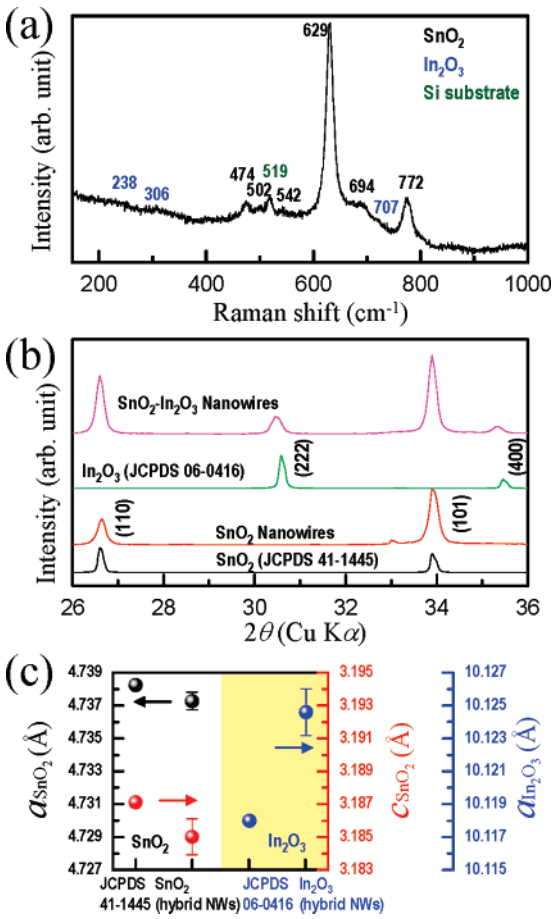

Figure 3. (a) Room-temperature Raman spectrum of $SnO_2-In_2O_3$ nanowires. (b) X-ray diffraction patterns of $SnO_2-In_2O_3$ and SnO_2 nanowires. (c) Lattice parameters of $SnO_2-In_2O_3$ nanowires given by the XRD pattern in (b).

During the tip-led growth of the SnO_2 nanowires, it is expected that the In_2O_3 flux (oxidized In flux) is adsorbed onto the surface of the SnO_2 nanowires rather than their tips. The nucleation and growth aspects of the In_2O_3 shell structure are illustrated schematically in panels a−c of Figure 2. After it reaches the thermodynamic size limit, whether the In_2O_3 nucleus forms in an anisotropic (Figure 2b) or isotropic manner (Figure 2c) is determined by the free energy gain during the formation process (refer to the Supporting Information). In this case, the free energy gain when it forms in an anisotropic manner is lower than that when it forms in an isotropic manner (prism-shaped nucleus). The nuclei of In_2O_3 grow in an anisotropic manner in the early stages of the growth of the SnO_2/In_2O_3 core/shell nanostructures (Figure 1e). The nucleus continues to grow in an anisotropic manner, while conserving its prism shape afforded by the anisotropic growth mechanism, until it meets another nucleus. The resulting contiguous nuclei array is then transformed into a shell satisfying the flat-filling growth manner rather than the saw-filling growth manner. The selection of the growth manner is governed by the difference in the surface energies of the In_2O_3 nucleus and the SnO_2 core. The flat-filling growth manner can be rationalized by the observation of an In_2O_3 shell structure that is parallel to the SnO_2 nanowire (panels d and g of Figure 1). The details of the growth mechanism are demonstrated further in the Supporting Information.

During the formation of the In_2O_3 shell structure, the incorporation of Sn atoms into the In_2O_3 lattice structure deserves more discussion. Figure 3a shows the room-temperature Raman spectrum of the $SnO_2-In_2O_3$ heterostructure. Three normal phonon modes, E_g, A_{1g}, and B_{2g}, which usually appear in the spectra of bulk polycrystalline SnO_2 with a tetragonal structure, are detected at frequency shifts of 474, 629, and 772 cm^{-1}, respectively.[29] In addition to these classical modes, three abnormal Raman lines are observed in the spectrum at 502, 542, and 694 cm^{-1}, respectively, which were also detected in the Raman spectra of nanostructured SnO_2.[30,31] The weak Raman shifts at 238, 306, and 707 cm^{-1} can be ascribed to the presence of cubic In_2O_3.[32] The presence of composite $SnO_2-In_2O_3$ phases is indicated by the XRD pattern, as expected (Figure 3b). The XRD pattern taken from the SnO_2 nanowires is in good agreement with the reported one (JCPDS, No. 41-1445). However, it is necessary to point out that the peak shift of SnO_2 is negligible, whereas the peaks corresponding to In_2O_3 shift to a lower 2θ angle in the spectrum of the $SnO_2-In_2O_3$ nanowires. The lattice parameters of each phase in the $SnO_2-In_2O_3$ nanowires deduced from the Rietveld refinement of

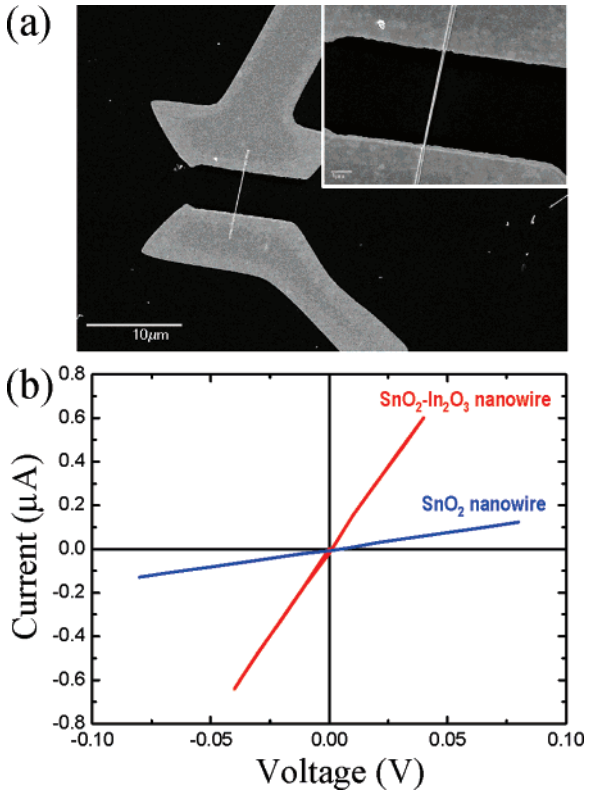

Figure 4. (a) SEM image of an individual $SnO_2-In_2O_3$ nanowire contacted by two metal electrodes. (b) Room-temperature $I-V$ characteristics of an individual $SnO_2-In_2O_3$ and SnO_2 nanowire.

the X-ray diffraction pattern are plotted in Figure 3c. The reported and calculated lattice parameters of SnO_2 show good agreement, but we observed a considerable increase in the lattice parameter of In_2O_3 in the $SnO_2-In_2O_3$ nanowires, which results from the tin doping in the In_2O_3 lattice. The calculated lattice parameter (a) of 10.125 Å is consistent with that of 6 atom % Sn-doped In_2O_3, which is known to be the solubility limit of tin in In_2O_3 without the presence of $In_4Sn_3O_{12}$ second phase.[33] Although further, more exact investigation of the doping content is needed, our result implies that considerable Sn incorporation into the In_2O_3 lattice occurs during the nucleation and growth of the In_2O_3 shell nanostructrues.

We carried out electron transport measurements on an individual $SnO_2-In_2O_3$ nanowire, as exemplified in Figure 4. The conductivity of the pure SnO_2 nanowire was found to be 2.76 S/cm at room temperature, which is similar to the values previously reported for other individual nanowires.[34,35] Significantly, the estimated conductivity of the $In_2O_3-SnO_2$ nanowire was 145.5 S/m, which is 2 orders of magnitude better than that of the pure SnO_2 nanowire. Sn-doped In_2O_3 (ITO) has become by far the most important transparent conducting oxide material. Wan et al. reported recently that the conductivity of individual ITO nanowires was 1089.3 S/cm, whereas that of In_2O_3 nanowires without intentional doping is of the order of 1 S/cm.[36] Therefore, the high conductivity of the $SnO_2-In_2O_3$ nanowire could be attributed to the formation of the ITO shell nanostructure caused by the effective incorporation of Sn into the In_2O_3 lattice, as described in Figure 3.

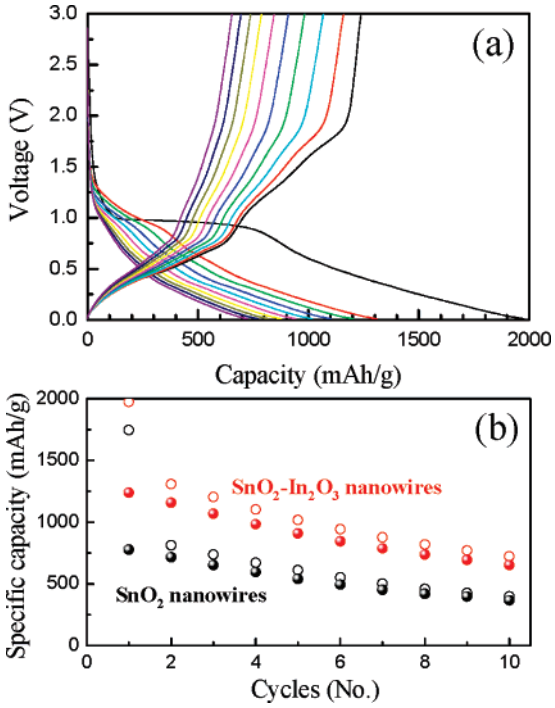

Figure 5. (a) Charging−discharging curves for the $SnO_2-In_2O_3$ nanowires/Li half-cell cycled between 3 and 0.01 V at a rate of $C/5$. (b) Variation in discharge−charge specific capacity vs cycle number for the $SnO_2-In_2O_3$ and SnO_2 nanowires.

High-performance Li-ion batteries require not only fast Li insertion/deinsertion but also high electronic conduction to facilitate efficient charging. To evaluate the electrochemical performance of our nanowire heterostructure, the voltage/specific capacity curves were obtained for the $SnO_2-In_2O_3$ nanowires/Li half-cell and its behavior is shown in Figure 5a. The cell was cycled at a rate of $C/5$ (here, C was defined as 4.4 Li ions per hour per formula unit of SnO_2).[17] During the first discharge, the voltage drops rapidly and reaches a plateau at ~0.97 V, reflecting the formation of Li_2O based on the irreversible reaction, $SnO_2 + 4Li \rightarrow Sn + 2Li_2O$, and then decreases gradually to 0.01 V.

As previously reported, the specific capacity of SnO_2 nanostructures (nanoparticles, nanowires, nanorods, and nanotubes) depends strongly on their size and morphology.[19−21,37,38] We confirmed the dependency of the capacity of the various SnO_2 nanowires prepared at different temperatures on their size (especially their diameter), under the same electrochemical test condition (data not shown). On the basis of these observations, pure SnO_2 nanowires comparable in diameter to the $SnO_2-In_2O_3$ nanowires were examined under the same conditions for the purpose of comparison (Figure S2). The $SnO_2-In_2O_3$ heterostructured nanowires exhibited a higher initial and reversible lithium storage capacity than the pure SnO_2 nanowires (Figure 5b). A first discharge capacity of 1975 mA h/g and a reversible capacity of ~700 mA h/g after 10 cycles were observed for the $SnO_2-In_2O_3$ nanowires.

It has been suggested that the capacity of 1D nanomaterials is improved by the facility of Li ion diffusion afforded by their large surface-to-volume ratio and high crystallinity.[12−16] The additional lithium storage capacity in $SnO_2-In_2O_3$

nanowires may result from the Li reactivity of the Sn-doped In_2O_3 (ITO) shell. Inductively coupled plasma mass spectroscopy analysis revealed that the mass ratio of Sn:In was 0.67:0.33. For the purpose of comparison, we evaluated the half-cells made from the In_2O_3 and In powders under the same electrochemical test conditions. Although the first discharge capacity of the In_2O_3 powder is quite large, namely, ~1450 mA h/g, its reversible capacity is negligible even after two cycles (Figure S3). Additionally, we observed that the In powder is electrochemically inactive based on the same galvanostatic cycling. Indeed, we did not observe the formation of In−Li imtermetallic compounds in the ex situ XRD patterns of the In_2O_3 powders collected in the fully discharged state after five cycles (Figure S4). Only In and Li_2O phases were identified in the discharged state, which proves the reduction of In_2O_3 to metallic In by the reaction $In_2O_3 + 6Li \rightarrow 2In + 3Li_2O$, corresponding to the high first irreversible discharge capacity.

Such findings suggest another consideration regarding the high lithium storage capacity of the $SnO_2-In_2O_3$ nanowires. More recently, it was reported that the incorporation of Au clearly enhanced the reversible capacity of Co_3O_4 nanowires due to the conductive and catalytic effects of the Au nanoparticles on the reaction of Li with Co_3O_4.[15] Indeed, surface modification by depositing metals and metal oxides can improve the electrochemical performance, because the charge-transfer resistance is decreased.[39−41] The above-mentioned $SnO_2-In_2O_3$ nanowires have excellent electronic conductivity. In addition, it is expected that the metallic In produced by the reduction of In_2O_3 may maintain the high conductivity of the nanowires during cycling. Although the exact electrochemical mechanism still remains unclear, our results show marked improvements in the electrochemical performance of the SnO_2 electrode afforded by the one-step deposited surface coating, leading to the production of highly conductive nanowires.

In summary, the one-step thermal evaporation process was used to produce SnO_2/In_2O_3 core/shell 1D nanostructures, which are formed due to the differences in the reactivities of the core and shell materials. This coaxial hetero-nanostructure formed by the growth of crystalline ITO overlayers on the core SnO_2 nanowires offers enhanced electronic conductivity, which is important for Li ion battery electrodes. The details of the nucleation and growth aspects of the $SnO_2-In_2O_3$ nanowires are represented schematically. Our result demonstrates that the specific capacity of $SnO_2-In_2O_3$ nanowires is estimated to be at least 60% greater than that of our pure SnO_2 nanowires. Additionally, we anticipate that this ability to obtain highly conductive nanowires allows for their potential application to solar cells, field emitters, and gas sensors.

Supporting Information Available: Images showing the SnO_2/In_2O_3 core/shell heterostructure, a schematic representation of nanowire growth, FESEM images of SnO_2 nanowires prepared at different temperatures, charge discharge curves for In_2O_3 powders, and ex situ XRD patterns and discussion of theoretical analysis of the growth mechanism of $SnO_2-In_2O_3$ heterostructured nanowires This material is available free of charge via the Internet at http://pubs.acs.org.

References

(1) Rao, C. N. R.; Deepak, F. L.; Gundiah, G.; Govindaraj, A. *Prog. Solid State Chem.* **2003**, *31*, 5.
(2) Lieber, C. M.; Wang, Z. L. *MRS Bull.* **2007**, *32*, 99.
(3) Lauhon, L. J.; Gudiksen, M. S.; Wang, D.; Lieber, C. M. *Nature* **2002**, *420*, 57.
(4) Ha, B.; Kim, H. C.; Kang, S. G.; Kim, Y. H.; Lee, J. Y.; Park, C. Y.; Lee, C. J. *Chem. Mater.* **2005**, *17*, 5398.
(5) Park, W. I.; Yoo. J.; Kim, D. W.; Yi, G. C.; Kim, M. *J. Phys. Chem. B* **2006**, *110*, 1516.
(6) Zhou, J.; Liu, J.; Wang, X.; Song, J.; Tummala, R.; Xu, N. S.; Wang, Z. L. *Small* **2007**, *3*, 622.
(7) Yin, Y.; Lu, Y.; Sun, Y.; Xia, Y. *Nano Lett.* **2002**, *2*, 427.
(8) Hsu, Y. J; Lu, S. Y. *Chem. Commun.* **2004**, 2102.
(9) Xiang, J.; Lu, W.; Hu, Y.; Wu, Y.; Yan, H.; Lieber, C. M. *Nature* **2006**, *441*, 489.
(10) Ouyang, L.; Maher, K. N.; Yu, C. L.; McCarty, J.; Park, H. *J. Am. Chem. Soc.* **2007**, *129*, 133.
(11) Mieszawska, A. J.; Jalilian, R.; Sumanasekera, G. U.; Zamborini, F. P. *Small* **2007**, *3*, 722.
(12) Sides, C. R.; Martin, C. R. *Adv. Mater.* **2005**, *17*, 125.
(13) Armstrong, A. R.; Armstrong, G.; Canales, J.; Garcia, R.; Bruce, P. G. *Adv. Mater.* **2005**, *17*, 862.
(14) Cheng, F.; Chen, J. *J. Mater. Res.* **2006**, *21*, 2744.
(15) Nam, K. T.; Kim, D. W.; Yoo, P. J.; Chiang, C. Y.; Meethong, N.; Hammond, P. T.; Chiang, Y. M.; Belcher, A. M. *Science* **2006**, *312*, 885.
(16) Chan, C. K.; Peng, H.; Twesten, R. D.; Jarausch, K.; Zhang, X. F.; Cui, Y. *Nano Lett.* **2007**, *7*, 490.
(17) Courtney, I. A.; Dahn, J. R. *J. Electrochem. Soc.* **1997**, *144*, 2045.
(18) Brousse, T.; Retoux, R.; Herterich, U.; Schleich, D. M. *J. Electrochem. Soc.* **1998**, *145*, 1.
(19) Wang, Y.; Lee, J. Y. *J. Phys. Chem. B* **2004**, *108*, 17832.
(20) Ying, Z.; Wan, Q.; Cao, H.; Song, Z. T.; Feng, S. L. *Appl. Phys. Lett.* **2005**, *87*, 113108.
(21) Park, M. S.; Wang, G. X.; Kang, Y. M.; Wexler, D.; Dou, S. X.; Liu, H. K. *Angew. Chem., Int. Ed.* **2007**, *46*, 750.
(22) Guyomar, D.; Tarascon, J. M. *J. Electrochem. Soc.* **1993**, *140*, 3071.
(23) Wang, J. X.; Chen, H. Y.; Gao, Y.; Liu, D. F.; Song, L.; Zhang, Z. X.; Zhao, X. W.; Dou, X. Y.; Luo, S. D.; Zhou, W. Y.; Wang, G.; Xie, S. S. *J. Cryst. Growth* **2005**, *284*, 73.
(24) Wang, J.; Xie, S.; Zhou, W. *MRS Bull.* **2007**, *32*, 123.
(25) Shackelford, J. F.; Alexander, W. *Materials Science and Engineering Handbook*, 3rd ed.; CRC Press: New York, 2001.
(26) Liu, Q. X.; Wang, C. X.; Xu, N. S.; Wang, G. W. *Phys. Rev. B* **2005**, *72*, 085417.
(27) Kwon, S. J.; Park, J. G. *J. Phys.: Condens. Matter* **2006**, *18*, 3875.
(28) Kwon, S. J. *J. Phys. Chem. B* **2006**, *110*, 3876.
(29) Peercy, P. S.; Morosin, B. *Phys. Rev. B* **1973**, *7*, 2779.
(30) Abello, L.; Bochu, B.; Gaskov, A.; Koudryavtseva, S.; Lucazeau, G.; Roumyantseva, M. *J. Solid State Chem.* **1998**, *135*, 78.
(31) Liu, Y.; Liu, M. *Adv. Funct. Mater.* **2005**, *15*, 57.
(32) White, W. B.; Keramidas, V. G. *Spectrochim. Acta* **1972**, *28*, 501.
(33) Nadaud, N.; Lequeux, N.; Nanot, M.; Jové, J.; Roisnel, T. *J. Solid State Chem.* **1998**, *135*, 140.
(34) Ma, Y. J.; Zhou, F.; Lu, L.; Zhang, Z. *Solid State Commun.* **2004**, *130*, 313.
(35) Hernández-Ramírez, F.; Taranscón, A.; Casals, O.; Rodríguez, J.; Romano-Rodríguez, A.; Morante, J. R.; Barth, S.; Mathur, S.; Choi, T. Y.; Poulikakos, D.; Callegari, V.; Nellen, P. M. *Nanotechnology* **2006**, *17*, 5577.
(36) Wan, Q.; Dattoli, E. N.; Fung, W. Y.; Guo, W.; Chen, Y.; Pan, X.; Lu, W. *Nano Lett.* **2006**, *6*, 2909.
(37) Kim, C.; Noh, M.; Choi, M.; Cho, J.; Park, B. *Chem. Mater.* **2005**, *17*, 3297.
(38) Wang, Y.; Lee, J. Y.; Zeng, H. C. *Chem. Mater.* **2005**, *17*, 3899.
(39) Yuan, L.; Konstantinov, K.; Wang, G. X.; Liu, H. K.; Dou, S. X. *J. Power Sources* **2005**, *146*, 180.
(40) Fu, L. J.; Liu, H.; Li, C.; Wu, Y. P.; Rahm, E.; Holze, R.; Wu, H. Q. *Solid State Sci.* **2006**, *8*, 113.
(41) Ellis, B.; Herle, P. S.; Rho, Y. H.; Nazar, L. F.; Dunlap, R.; Perry, L. K.; Ryan, D. H. *Faraday Discuss.* **2007**, *134*, 119.

NL0715037